Phonon-assisted spin-polarized tunneling through an interacting quantum dot

2008 J. Phys.: Condens. Matter 20 275214

(http://iopscience.iop.org/0953-8984/20/27/275214)

IOP PUBLISHING JOURNAL OF PHYSICS: CONDENSED MATTER

J. Phys.: Condens. Matter **20** (2008) 275214 (10pp) doi:10.1088/0953-8984/20/27/275214

Phonon-assisted spin-polarized tunneling through an interacting quantum dot

W Rudziński

Department of Physics, Adam Mickiewicz University, ulica Umultowska 85, 61-614 Poznań, Poland

E-mail: wojrudz@amu.edu.pl

Received 12 February 2008, in final form 21 April 2008
Published 4 June 2008
Online at stacks.iop.org/JPhysCM/20/275214

Abstract

Using the nonequilibrium Green function technique we study theoretically spin-polarized transport in double-barrier tunneling junctions based on a single-level quantum dot interacting with a local phonon mode. Phonon emission and absorption spectra have been calculated for arbitrary Coulomb correlations on the dot and for different temperatures. It is shown that in the nonlinear response regime the electron–phonon interaction gives rise to current suppression in symmetric junctions as well as to oscillations of the tunnel magnetoresistance (TMR). In asymmetric junctions, the same mechanism may lead effectively to enhancement of the diode-like characteristics. We have also found that at sufficiently low temperatures additional phonon-induced resonance peaks appear in the linear spectral function on both sides of the main resonance peaks corresponding to the quantum dot energy levels. The case of negative effective charging energy is also analyzed numerically. A significant enhancement of electric current (or suppression of TMR) above the threshold bias voltages at which the dot energy level enters the tunneling window is observed. The gate voltage-controlled rectification effect of the tunneling current in asymmetric junctions with positive and negative effective Coulomb correlations is also discussed.

(Some figures in this article are in colour only in the electronic version)

1. Introduction

Electronic transport through discrete levels of single molecules, carbon nanotubes or quantum dots (QDs) coupled to vibrational degrees of freedom has been investigated recently in a number of experimental [1–10], as well as theoretical works [11, 13–27]. In particular, it is reported that the nonresonant tunneling of electrons in single-molecule transistors is associated with excited vibrational modes of the molecule. Thus, if the electron–phonon coupling is sufficiently large then the tunneling electron can absorb or emit phonons, altering its energy, which consequently may influence significantly the current–voltage (I–V) characteristics. It is observed that in addition to the resonant peak associated with the discrete level of the dot, satellite peaks separated at the phonon mode frequency also appear in the differential conductance (see e.g. [1, 3, 7, 9]). In single-molecule transistors inelastic cotunneling processes have been also identified with vibrational quanta of the molecule [10]. The same experiment shows that when the molecule contains an unpaired electron, then vibrational satellite features around the Kondo resonance are observed. A coherent interplay between single-electron tunneling and the excitation of localized phonon modes has been also demonstrated for rigid structures of semiconductor quantum dots. It was realized by investigating transport features of electron–phonon cavities with quantum dots embedded in a freestanding GaAs/AlGaAs membrane [8].

Up to now, the polaronic transport through molecular QDs has been studied theoretically mostly for non-magnetic tunneling junctions based on quantum dots with vanishing or infinite charging energy. The interplay between the electron–phonon interactions and arbitrary Coulomb correlations on the dot coupled to metallic electrodes has been studied in more detail by Galperin *et al* in [26]. In turn, transport properties of a QD with a negative effective charging energy have been better understood when, besides single-electron cotunneling, also electron pair-tunneling processes have been assumed to occur in the Coulomb blockade regime [22]. Very recently, tunnel magnetoresistance and Kondo phenomena have been investigated for the dot coupled to magnetic electrodes [25].

Numerical analysis of Wang *et al* [25] was mainly focused on calculation of spin-dependent density of states as a function of incident electron energy at zero bias voltage. It is shown that a set of new peaks induced by the phonon emission may appear on both sides of the main Kondo peak. Moreover, phonon-induced oscillatory behavior of the tunnel magnetoresistance has been predicted in extreme cases of large and vanishing Coulomb correlations on dots coupled to equivalent external electrodes.

The present work extends studies on phonon-assisted electronic transport in mesoscopic systems to the case of tunneling through a single-level quantum dot with arbitrary Coulomb correlations, coupled symmetrically or asymmetrically to ordinary ferromagnetic or half-metallic electrodes. One of the most widely studied spin-dependent effects in such magnetic tunnel junctions is the tunnel magnetoresistance (TMR). This phenomenon appears as a change in the junction resistance when magnetic moments of external electrodes are switched between the parallel alignment and the antiparallel one. The TMR effect is known to occur in planar junctions [28–30], mesoscopic double-barrier junctions [31–35, 38–46] as well as in granular systems [47, 48].

In this paper, TMR is analyzed numerically in a context of polaronic transport through an interacting quantum dot (or a molecule). We assume arbitrary Coulomb correlations on the dot and the cases of both positive and negative effective charging energy induced by the polaron shift are taken into account. It is also assumed that to form a polaron, the strength of electron–phonon interactions is large compared to the tunneling rates. Such assumptions allow us to derive self-consistent integrals for the occupation numbers on the dot by using the nonequilibrium Green function technique based on equation of motion combined with a canonical Lang–Firsov transformation, known from the so-called independent boson model [49].

Several theoretical approaches, within the nonequilibrium Green function technique, have been used recently to describe the phonon-assisted tunneling through molecular QDs. This stimulated a discussion over two different results due to different approximations applied in calculating the Green function correlators for the system. One result is that due to phonon emission at low temperatures phonon satellites in the spectral function appear only on one side of the main elastic peak. As shown first by Flensberg [16] and later by Chen *et al* [20], the approximation of the Green function correlators by electron (or holes) contributions only [11, 13–15, 17], leading to such a behavior, is valid only at high temperatures and (or) when electrons (or holes) are sufficiently far from the Fermi surface, or in the weak tunneling limit. The latter dot-lead coupling regime has been realized in recent experiments on localized phonon excitations for quantum dots weakly coupled to the source and drain contacts [3, 8]. As stated in [8] these measurements may be related to theoretical predictions [11, 13–17] for transport through a molecular single-electron transistor coupled to a single-vibrational mode. These models have also been extended in order to analyze the origin of the blockade mechanism as well as the effect of Rabi oscillation-like coherent emission–reabsorption of the phonon mode, observed in the linear transport regime for a suspended quantum dot in a phonon cavity.

The other result is that one observes phonon satellites on both sides of the main resonance peak due to considering both the electron and hole contributions [24–26]. In our present discussion, the effects due to both the electron and hole transport are included and all the Green function correlators are derived on an equal footing by means of the equation of motion method applied for nonequilibrium Green functions in the Hartree–Fock approximation. Thus, the Kondo resonance effects are beyond the applicability of our approach and these will be reported elsewhere within other approximations. We extend the recent studies on electron–phonon interactions in magnetic tunnel junctions by calculating phonon emission and absorption spectra for arbitrary (positive or negative) effective charging energies on the dot. The consequences of the polaron shift on the electric current as well as on the corresponding differential conductance are then analyzed for a more general case of empty, single or doubly occupied dot. The resulting modifications of TMR are displayed and discussed in both the linear as well as nonlinear response regimes. The mechanism leading to oscillations of TMR, the origin of suppression of spin-polarized tunneling current in symmetric junctions as well as the origin of enhancement of the diode-like behavior in asymmetric junctions is explained in terms of phonon-assisted tunneling processes. We also reconsider studies on a negative effective charging energy in tunneling junctions. Here, properties of the TMR characteristics are discussed for a wide range of bias voltages and for both symmetric and asymmetric junctions.

The paper is organized as follows. In section 2 we describe the model of the system. The theoretical method is described in section 3, where the equation of motion method is used to derive nonequilibrium Green functions of the dot. Next, the Green functions are used to calculate transport characteristics for the system. Relevant numerical results for spectral functions, tunneling current, conductance as well as magnetoresistance are presented and discussed in section 4. Finally, a summary and general conclusions are in section 5.

2. Model

We consider a single-level QD coupled to two ferromagnetic metallic leads by tunneling barriers. The whole system can be described by a Hamiltonian of the general form

$$H = H_{\mathrm{l}} + H_{\mathrm{r}} + H_{\mathrm{ph}} + H_{\mathrm{d}} + H_{\mathrm{t}}. \tag{1}$$

The term H_ν describes the left ($\nu = \mathrm{l}$) and right ($\nu = \mathrm{r}$) electrodes in the non-interacting quasi-particle approximation,

$$H_\nu = \sum_{k,\sigma} \varepsilon^{\nu}_{k\sigma} a^{+}_{\nu k\sigma} a_{\nu k\sigma}, \tag{2}$$

where $\varepsilon^{\nu}_{k\sigma}$ is the single-electron energy in the νth electrode for the wavevector k and spin σ ($\sigma = \uparrow, \downarrow$), whereas $a^{+}_{\nu k\sigma}$ and $a_{\nu k\sigma}$ are the corresponding creation and annihilation operators. The second term is the phonon Hamiltonian:

$$H_{\mathrm{ph}} = \omega_0 b^{+} b, \tag{3}$$

where ω_0 is the vibrational frequency of the phonon mode and b^+ (b) is the phonon creation (annihilation) operator. The term H_d in equation (1) describes QD,

$$H_\mathrm{d} = \sum_\sigma [\varepsilon_\mathrm{d} + eV_\mathrm{g} + \lambda(b + b^+)]c_\sigma^+ c_\sigma + Un_\uparrow n_\downarrow, \quad (4)$$

where ε_d denotes the energy of the discrete level, which may be controlled by the gate voltage V_g, U is the electron correlation parameter, the parameter λ describes strength of the electron–phonon coupling, c_σ^+ and c_σ is the creation and annihilation operator, respectively, for electrons with spin orientation $\sigma = \uparrow (\downarrow)$, whereas $n_\sigma = c_\sigma^+ c_\sigma$ is the occupation operator. Finally, the tunneling term, H_t, in equation (1) takes the form

$$H_\mathrm{t} = \sum_{\nu,k,\sigma} T_{k\sigma}^\nu a_{\nu k\sigma}^+ c_\sigma + \mathrm{H.c.}, \quad (5)$$

where $T_{k\sigma}^\nu$ ($\nu = l, r$) is the tunneling amplitude, and H.c. stands for the Hermitian conjugate terms.

Now, it is useful to eliminate the linear coupling terms in the Hamiltonian H_d by using the following Lang–Firsov-type unitary transformation [49]:

$$\widetilde{H} = \mathrm{e}^S H \mathrm{e}^{-S}, \qquad S = \frac{\lambda}{\omega_0} c_\sigma^+ c_\sigma (b^+ - b). \quad (6)$$

With this transformation the fermion and boson operators read

$$\widetilde{c}_\sigma = c_\sigma X, \quad (7)$$

$$\widetilde{c}_\sigma^+ = c_\sigma^+ X^+, \quad (8)$$

$$\widetilde{b} = b - \sum_\sigma \frac{\lambda}{\omega_0} c_\sigma^+ c_\sigma, \quad (9)$$

$$\widetilde{b}^+ = b^+ - \sum_\sigma \frac{\lambda}{\omega_0} c_\sigma^+ c_\sigma, \quad (10)$$

where X is the phonon operator, $X = \exp[-(\lambda/\omega_0)(b^+ - b)]$. Thus, the Hamiltonian (1) is reshaped into the following form

$$\widetilde{H} = H_\nu + H_\mathrm{ph} + \widetilde{H}_\mathrm{d} + \widetilde{H}_t, \quad (11)$$

where

$$\widetilde{H}_\mathrm{d} = \sum_\sigma \widetilde{\varepsilon}_\mathrm{d} c_\sigma^+ c_\sigma + \widetilde{U} n_\uparrow n_\downarrow, \quad (12)$$

with the renormalized dot energy level, $\widetilde{\varepsilon}_\mathrm{d} = \varepsilon_\mathrm{d} + eV_\mathrm{g} - \lambda^2/\omega_0$, and with the renormalized charging energy, $\widetilde{U} = U - 2\lambda^2/\omega_0$. The tunneling matrix elements are also renormalized,

$$\widetilde{H}_t = \sum_{\nu,k,\sigma} \widetilde{T}_{k\sigma}^\nu a_{\nu k\sigma}^+ c_\sigma + \mathrm{H.c.}, \quad (13)$$

where $\widetilde{T}_{k\sigma}^\nu = T_{k\sigma}^\nu X$.

Assuming that the local polaron is localized, i.e. assuming that hopping is small compared to electron–phonon interactions, $T_{k\sigma}^\nu \ll \lambda$ (same approach as e.g. in [16, 20, 25]), we adopt here the approximation developed for the independent boson model [49], and replace the phonon operator X in equation (13) with its expectation value, $\langle X \rangle = \exp[-(\lambda/\omega_0)^2(N_\mathrm{ph} + 1/2)]$, where N_ph is the Bose distribution, $N_\mathrm{ph} = 1/[\exp(\beta\omega_0) - 1]$, and $\beta = 1/k_\mathrm{B}T$. Thus, exponential suppression of the tunneling amplitudes in the tunneling Hamiltonian (13) arises, which in turn leads to the charge conserving λ-dependent Franck–Condon blockade of tunneling processes between the dot and an external electrode. As mentioned, this situation is valid until the tunneling amplitude does not depend on the polaron position. In a recent theoretical attempt at going beyond the independent boson model for a non-magnetic molecular tunneling junction, it has been shown that when intramolecular vibrations of a longer lifetime take place then an additional renormalization of the phonon subsystem due to coupling to a tunneling electron occurs [24]. The latter case is omitted in the present paper. The situation considered here applies mainly to structures similar to those realized experimentally so far, in which a dependence of tunneling rates on the oscillator position is negligible (see e.g. [8]).

3. Green function formalism

To calculate electric current in the nonequilibrium situation we make use of the nonequilibrium Green function defined on the Keldysh contour [12]. Accordingly, we introduce the causal (time-ordered) Green function of the dot, $G_{\sigma\sigma'}(t) \equiv -\mathrm{i}\langle T[c_\sigma(t)\, c_{\sigma'}^+(0)]\rangle$, as well as the lesser and greater correlation Green function defined as $G_{\sigma\sigma'}^<(t) \equiv \mathrm{i}\langle c_{\sigma'}^+(0) c_\sigma(t)\rangle$ and $G_{\sigma\sigma'}^>(t) \equiv -\mathrm{i}\langle c_\sigma(t) c_{\sigma'}^+(0)\rangle$, respectively. From the canonical transformation given by equations (7) and (8) it follows that the time-ordered Green function may be separated into the electron and phonon correlators:

$$\begin{aligned} G_{\sigma\sigma'}(t) &= \left[-\mathrm{i}\theta(t)\langle c_\sigma(t)\, c_{\sigma'}^+(0)\rangle + \mathrm{i}\theta(-t)\langle c_{\sigma'}^+(0)\, c_\sigma(t)\rangle\right] \\ &\quad \times \langle X(t)\, X^+(0)\rangle + \mathrm{i}\theta(-t)\langle c_{\sigma'}^+(0)\, c_\sigma(t)\rangle \\ &\quad \times \left\langle \left[X^+(0)X(t) - X(t)X^+(0)\right]\right\rangle \\ &= \widetilde{G}_{\sigma\sigma'}(t)\langle X(t)X^+(0)\rangle + \theta(-t)\widetilde{G}_{\sigma\sigma'}^<(t)\left\langle \left[X^+(0), X(t)\right]_-\right\rangle, \end{aligned} \quad (14)$$

with $\widetilde{G}_{\sigma\sigma'}(t)$ and $\widetilde{G}_{\sigma\sigma'}^<(t)$ being the so-called dressed correlators for the system governed by the transformed Hamiltonian (11). Thermodynamic averaging of the phonon correlators $\langle X(t)\, X^+(0)\rangle$ and $\langle X^+(0)\, X(t)\rangle$ over the phonon distributions results in the following expression for the undressed lesser (greater) Green function $G_{\sigma\sigma'}^{<(>)}(t)$:

$$G_{\sigma\sigma'}^{<(>)}(t) = \widetilde{G}_{\sigma\sigma'}^{<(>)}(t) \exp[-\phi(\mp t)]. \quad (15)$$

where the quantity $\phi(t)$ is given by [49]

$$\phi(t) = \left(\frac{\lambda}{\omega_0}\right)^2 \left[N_\mathrm{ph}(1 - \mathrm{e}^{\mathrm{i}\omega_0 t}) + (N_\mathrm{ph} + 1)(1 - \mathrm{e}^{-\mathrm{i}\omega_0 t})\right]. \quad (16)$$

If we expand $\exp[\mp\phi(t)]$ in a power series in $\exp(\mathrm{i}\omega_0 t)$, then using Bessel functions of complex argument, $I_n(z)$, equation (16) can be rewritten as:

$$\exp[\mp\phi(t)] = \sum_{n=-\infty}^{+\infty} L_n \mathrm{e}^{\mp \mathrm{i}n\omega_0 t}, \quad (17)$$

with

$$L_n = \mathrm{e}^{-\left(\frac{\lambda}{\omega_0}\right)^2}\left(\frac{\lambda}{\omega_0}\right)^{2n}\left(\frac{1}{n!}\right) \tag{18}$$

for $T = 0$ and

$$L_n = \mathrm{e}^{-(\frac{\lambda}{\omega_0})^2(2N_{\mathrm{ph}}+1)}\mathrm{e}^{\frac{n\omega_0\beta}{2}} I_n\left[2\left(\frac{\lambda}{\omega_0}\right)^2\sqrt{N_{\mathrm{ph}}(N_{\mathrm{ph}}+1)}\right] \tag{19}$$

for $T > 0$.

The explicit expression for the dressed Green functions $\widetilde{G}_{\sigma\sigma'}(t)$ and $\widetilde{G}^{<(>)}_{\sigma\sigma'}(t)$ can be obtained by using the equation of motion method. The equation of motion for the Fourier transforms of the causal and lesser (greater) correlators defined as $\widetilde{G}_{\sigma\sigma'}(\epsilon) \equiv \langle\langle c_\sigma \,|\, c^+_{\sigma'}\rangle\rangle_\epsilon$ and $\widetilde{G}^{<(>)}_{\sigma\sigma'}(\epsilon) \equiv \langle\langle c_\sigma \,|\, c^+_{\sigma'}\rangle\rangle^{<(>)}_\epsilon$, respectively, read (see e.g. [37])

$$\begin{aligned}(\epsilon - \widetilde{\epsilon}_d)\langle\langle c_\sigma \,|\, c^+_{\sigma'}\rangle\rangle_\epsilon &= \delta_{\sigma\sigma'} \\ &+ \sum_k\left[\widetilde{T}^{*l}_{k\sigma}\langle\langle a_{lk\sigma} \,|\, c^+_{\sigma'}\rangle\rangle_\epsilon + \widetilde{T}^{*r}_{k\sigma}\langle\langle a_{rk\sigma} \,|\, c^+_{\sigma'}\rangle\rangle_\epsilon\right] \\ &+ \widetilde{U}\langle\langle c_\sigma n_{-\sigma} \,|\, c^+_{\sigma'}\rangle\rangle_\epsilon, \end{aligned} \tag{20}$$

$$\begin{aligned}(\epsilon - \widetilde{\epsilon}_d)\langle\langle c_\sigma \,|\, c^+_{\sigma'}\rangle\rangle^{<(>)}_\epsilon &= \sum_k\left[\widetilde{T}^{*l}_{k\sigma}\langle\langle a_{lk\sigma} \,|\, c^+_{\sigma'}\rangle\rangle^{<(>)}_\epsilon + \widetilde{T}^{*r}_{k\sigma}\langle\langle a_{rk\sigma} \,|\, c^+_{\sigma'}\rangle\rangle^{<(>)}_\epsilon\right] \\ &+ \widetilde{U}\langle\langle c_\sigma n_{-\sigma} \,|\, c^+_{\sigma'}\rangle\rangle^{<(>)}_\epsilon. \end{aligned} \tag{21}$$

Applying equation of motion to the three new Green functions on the rhs of equation (20), one finds

$$(\epsilon - \varepsilon^\nu_{k\sigma})\langle\langle a_{\nu k\sigma} \,|\, c^+_{\sigma'}\rangle\rangle_\epsilon = \widetilde{T}^\nu_{k\sigma}\langle\langle c_\sigma \,|\, c^+_{\sigma'}\rangle\rangle_\epsilon, \tag{22}$$

$$\begin{aligned}(\epsilon - \widetilde{\epsilon}_d - \widetilde{U})\langle\langle c_\sigma n_{-\sigma} \,|\, c^+_{\sigma'}\rangle\rangle_\epsilon &= \langle n_{-\sigma}\rangle \\ &+ \sum_{k\nu}\widetilde{T}^{*\nu}_{k\sigma}\langle n_{-\sigma}\rangle\langle\langle a_{\nu k\sigma} \,|\, c^+_{\sigma'}\rangle\rangle_\epsilon. \end{aligned} \tag{23}$$

In obtaining the equation of motion (23) for the higher-order Green function we have neglected correlations involving lead electrons and the Hartree–Fock decoupling scheme was applied, $\langle\langle a_{\nu k\sigma}\, n_{-\sigma} \,|\, c^+_{\sigma'}\rangle\rangle_\epsilon \rightarrow \langle n_{-\sigma}\rangle\langle\langle a_{\nu k\sigma} \,|\, c^+_{\sigma'}\rangle\rangle_\epsilon$, where $\langle\cdots\rangle$ means the quantum statistical average value of the appropriate operator. This approximation closes the set of equations (20), (22) and (23) allowing one to find a solution for the causal Green functions $\widetilde{G}_{\sigma\sigma'}(\epsilon)$:

$$\widetilde{G}_{\sigma\sigma}(\epsilon) = \frac{\epsilon - \widetilde{\varepsilon}_{\mathrm{d}} - \widetilde{U}(1 - \langle n_{-\sigma}\rangle)}{(\epsilon - \widetilde{\varepsilon}_{\mathrm{d}})(\epsilon - \widetilde{\varepsilon}_{\mathrm{d}} - \widetilde{U}) - [\epsilon - \widetilde{\varepsilon}_{\mathrm{d}} - \widetilde{U}(1 - \langle n_{-\sigma}\rangle)]\widetilde{\Sigma}_\sigma(\epsilon)}, \tag{24}$$

where $\widetilde{\Sigma}_\sigma(\epsilon)$ is the self-energy including contributions from the coupling to the leads,

$$\widetilde{\Sigma}_\sigma(\epsilon) = \sum_{k,\nu}\frac{|\widetilde{T}^\nu_{k\sigma}|^2}{\epsilon - \varepsilon^\nu_{k\sigma}}. \tag{25}$$

The retarded and advanced Green functions $\widetilde{G}^{\mathrm{R(A)}}_{\sigma\sigma}(\epsilon)$ can be found as $\widetilde{G}^{\mathrm{R(A)}}_{\sigma\sigma}(\epsilon) = \widetilde{G}_{\sigma\sigma}(\epsilon \pm \mathrm{i}\eta)$. Similarly, one can find $\widetilde{\Sigma}^{\mathrm{R(A)}}_\sigma(\epsilon)$. From equation (24) it follows that the retarded self-energy has the following form

$$\widetilde{\Sigma}^{\mathrm{R}}_\sigma(\epsilon) = -\sum_\nu\frac{1}{2}\widetilde{\Gamma}^\nu_\sigma(\epsilon)\left[\frac{1}{\pi}\ln\left(\frac{D + eV_\nu - \epsilon}{D - eV_\nu + \epsilon}\right) + i\right], \tag{26}$$

where

$$\widetilde{\Gamma}^\nu_\sigma(\epsilon) = \mathrm{e}^{-(\frac{\lambda}{\omega_0})^2(2N_{\mathrm{ph}}+1)}\Gamma^\nu_\sigma(\epsilon), \tag{27}$$

with

$$\Gamma^\nu_\sigma(\epsilon) = 2\pi\sum_k|T^\nu_{k\sigma}|^2\delta(\epsilon - \epsilon^\nu_{k\sigma}), \tag{28}$$

for $\nu = \mathrm{l}, \mathrm{r}$. It has been assumed that the lower and upper edges of the electron band at zero bias are at $-D$ and D, respectively.

In the following we assume

$$\Gamma^{\mathrm{l}}_{\uparrow(\downarrow)}(\epsilon) = \Gamma^{\mathrm{l}}_{\uparrow(\downarrow)} = \Gamma_0(1 \pm p_{\mathrm{l}}) \tag{29}$$

and

$$\Gamma^{\mathrm{r}}_{\uparrow(\downarrow)}(\epsilon) = \Gamma^{\mathrm{r}}_{\uparrow(\downarrow)} = \alpha\Gamma_0(1 \pm p_{\mathrm{r}}). \tag{30}$$

The parameters p_{l} and p_{r} describe the spin asymmetry of the coupling to the left and right electrodes, respectively, Γ_0 is a constant, and the parameter α takes into account asymmetry between coupling of the dot to the left and right electrodes.

Similarly, the correlation Green functions $\widetilde{G}^{<(>)}_{\sigma\sigma'}(\epsilon)$ can be found from the equation of motion (21):

$$\widetilde{G}^<_{\sigma\sigma'}(\epsilon) = -2\mathrm{i}\frac{f_{\mathrm{l}}(\epsilon)\Gamma^{\mathrm{l}}_\sigma + f_{\mathrm{r}}(\epsilon)\Gamma^{\mathrm{r}}_\sigma}{\Gamma^{\mathrm{l}} + \Gamma^{\mathrm{r}}}\,\mathrm{Im}\,\widetilde{G}^{\mathrm{R}}_{\sigma\sigma'}(\epsilon), \tag{31}$$

$$\widetilde{G}^>_{\sigma\sigma'}(\epsilon) = 2\mathrm{i}\frac{[1 - f_{\mathrm{l}}(\epsilon)]\Gamma^{\mathrm{l}}_\sigma + [1 - f_{\mathrm{r}}(\epsilon)]\Gamma^{\mathrm{r}}_\sigma}{\Gamma^{\mathrm{l}} + \Gamma^{\mathrm{r}}}\,\mathrm{Im}\,\widetilde{G}^{\mathrm{R}}_{\sigma\sigma'}(\epsilon), \tag{32}$$

where $f_\nu(\epsilon)$ is the Fermi–Dirac distribution function for the νth electrode, $f_\nu(\epsilon) = 1/\{1 + \exp[(\epsilon - \mu_\nu)/k_{\mathrm{B}}T]\}$, with the electrochemical potentials $\mu_{\mathrm{l}} = eV_{\mathrm{l}} = eV/2$ and $\mu_{\mathrm{r}} = eV_{\mathrm{r}} = -eV/2$. Note that the above equations (31) and (32) correspond exactly to the formulas presented in [20], obtained directly from the Keldysh equation for the correlator $\widetilde{G}^<_{\sigma\sigma'}(\epsilon)$.

The average values of the occupation numbers $\langle n_\sigma\rangle = \langle c^+_\sigma c_\sigma\rangle$, which enter the expressions for Green functions, have to be calculated self-consistently by using the formula

$$\langle n_\sigma\rangle = \mathrm{Im}\int_{-\infty}^{+\infty}\frac{\mathrm{d}\epsilon}{2\pi}G^<_{\sigma\sigma}(\epsilon), \tag{33}$$

which together with equations (15)–(19), (24) and (31) imply that

$$\begin{aligned}\langle n_\sigma\rangle = -\mathrm{Im}&\sum_{n=-\infty}^{+\infty}L_n \\ &\times\int_{-\infty}^{+\infty}\frac{\mathrm{d}\epsilon}{\pi}\left[\frac{\Gamma^{\mathrm{l}}_\sigma f_{\mathrm{l}}(\epsilon + n\omega_0) + \Gamma^{\mathrm{r}}_\sigma f_{\mathrm{r}}(\epsilon + n\omega_0)}{\Gamma^{\mathrm{l}}_\sigma + \Gamma^{\mathrm{r}}_\sigma}\right] \\ &\times\widetilde{G}^{\mathrm{R}}_{\sigma\sigma}(\epsilon + n\omega_0). \end{aligned} \tag{34}$$

Having found the Green functions, one can calculate the electric current flowing from the νth lead to the dot [50],

$$J_\nu = \frac{e}{\hbar}\int_{-\infty}^{+\infty}\frac{\mathrm{d}\epsilon}{2\pi}\mathrm{Tr}\left\{\mathbf{\Gamma}_\nu[\mathbf{G}^<(\epsilon) + f_\nu(\epsilon)\mathbf{A}(\epsilon)]\right\}, \tag{35}$$

where the quantity $\mathbf{A}_\sigma(\epsilon)$ stands for the spectral function,

$$\mathbf{A}_\sigma(\epsilon) = \mathrm{i}\left[G^>_{\sigma\sigma}(\epsilon) - G^<_{\sigma\sigma}(\epsilon)\right]. \tag{36}$$

Thus, the symmetrized expression for electric current, $J = (1/2)(J_l - J_r)$, finally reads

$$J = \frac{e}{h}\sum_{\sigma}\sum_{n=-\infty}^{+\infty} L_n \int_{-\infty}^{+\infty}\frac{d\epsilon}{2\pi}\{(\Gamma_\sigma^l[1-f_l(\epsilon)] - \Gamma_\sigma^r[1-f_r(\epsilon)])\widetilde{G}_{\sigma\sigma}^{<}(\epsilon+n\omega_0) + [\Gamma_\sigma^l f_l(\epsilon) - \Gamma_\sigma^r f_r(\epsilon)]\widetilde{G}_{\sigma\sigma}^{>}(\epsilon-n\omega_0)\} \quad (37)$$

whereas the corresponding TMR is given by:

$$\mathrm{TMR} = \frac{R_{AP}-R_P}{R_{AP}} = \frac{J_P - J_{AP}}{J_{AP}}, \quad (38)$$

where $J_{P(AP)}$ is the electric current flowing through the system when the spin polarizations of the leads are parallel (antiparallel).

4. Numerical results

In the following we shall discuss features of the polaronic transport through symmetric as well as asymmetric tunnel junctions. In the former case it is assumed that both barriers are identical, $\alpha = 1$, and the electrodes are made of the same ferromagnetic material, $p_l = p_r$. Regarding asymmetric junctions we take into account nonequivalent barriers, $\alpha \neq 1$, and assume that $p_l \neq p_r$. In particular, for numerical calculations we take $p_l = 0.4$, $p_r = 1$, and $\alpha = 0.1$. More specifically, it is assumed that the right electrode is made of a half-metallic material with electrons being totally spin-polarized at the Fermi level, whereas the factor $\alpha = 0.1$ indicates that on average electrons can tunnel much more easily to (from) the left electrode than to (from) the right one.

Note also that in discussion on nonlinear transport, the effective dot energy level is always assumed to be empty in the corresponding equilibrium situation, i.e. it is assumed that $\widetilde{\varepsilon}_d > 0$ at $V = 0$. Moreover, for clarity of our presentation, the spectral functions, the electric current as well as the corresponding conductance will be shown only for the parallel configuration of the magnetic moments of the external electrodes. The contribution from the antiparallel configuration is always present, according to equation (38), in the displayed TMR ratios. Finally note that the energy, temperature as well as the strength of the electron–phonon interaction λ is measured relative to the excitation energy ω_0.

4.1. Positive effective Coulomb energy, $\widetilde{U} > 0$

4.1.1. Linear response limit, $V = 0$. Consider first a symmetric tunneling junction in the equilibrium situation. Spectral functions for such a system, versus the energy ω are shown in figure 1. In the system where electron–phonon interactions are negligible, $\lambda = 0$, only the two resonance peaks (black solid curves) corresponding to the discrete level energies ε_d and $\varepsilon_d + U$ (note that $\widetilde{\varepsilon}_d = \varepsilon_d$ and $\widetilde{U} = U$ at $\lambda = 0$) are visible. The difference in height and width of these resonance peaks for up spin and down spin orientations indicates that one should expect down spin electrons to reside longer on the dot than up spin ones. It is worth noting here that qualitatively the same picture would be obtained for the antiparallel configuration, except that the spectral curves for opposite spin orientations would overlap. The latter follows from the fact that in symmetric junctions in the antiparallel configuration the dot may be occupied by up spin and down spin electrons with the same probability.

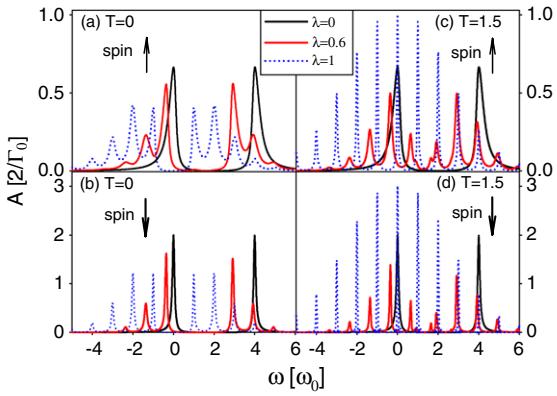

Figure 1. Spectral function versus energy ω calculated for selected values of the λ parameter. The spectral functions are plotted for two different temperatures, $T = 0$ ((a), (b)) and $T = 1.5$ ((c), (d)), and for the both electron spin polarizations in the parallel magnetic configuration of the junction. The parameters assumed for numerical calculations are: $\varepsilon_d = 0$, $U = 4$, $\Gamma_0 = 0.2$, $p_l = p_r = 0.5$, $V_g = 0$ and $\alpha = 1$.

When the electron–phonon interactions are switched on, the above picture becomes more complex depending on the strength of the electron–phonon coupling as well as on the temperature. With increasing strength of the electron–phonon coupling a shift of the elastic resonances down in energy occurs (see e.g. red solid lines in figure 1). The position of the left and right main resonance peaks in figure 1 corresponds to the renormalized energies $\widetilde{\varepsilon}_d$ and $\widetilde{\varepsilon}_d + \widetilde{U}$, respectively. Besides, as the curves calculated for $\lambda = 0.6$ show, satellite sidebands spaced at the phonon energies also appear in the spectral function. The satellite sidebands appearing on the right and left side of the main resonances originate from the particle and hole contributions, respectively. This implies that in a system near equilibrium, higher-order tunneling processes may be mediated by the phonon energy levels. Since at $T = 0$ there are no phonons to absorb, in figures 1(a) and (b) only peaks due to virtual phonon emission are visible.

With increasing temperature phonon absorption satellite peaks also appear, which are clearly seen in figures 1(c) and (d) below the resonance at $\widetilde{\varepsilon}_d$. Note also, that in the case considered of $\lambda = 0.6$ one still observes a significant reduction of the spectral function intensity with increasing temperature.

At sufficiently large λ the process of the polaron shift towards lower energies is accompanied by a dramatic change (see the blue dotted lines for $\lambda = 1$ in figure 1) in the spectral function. The resonance peaks become higher and narrower since, according to equation (27), with increasing value of the λ parameter the system is trapped in a region of exponentially suppressed transition rates. This behavior is even more prominent as the phonon population, N_{ph}, becomes larger with increasing temperature.

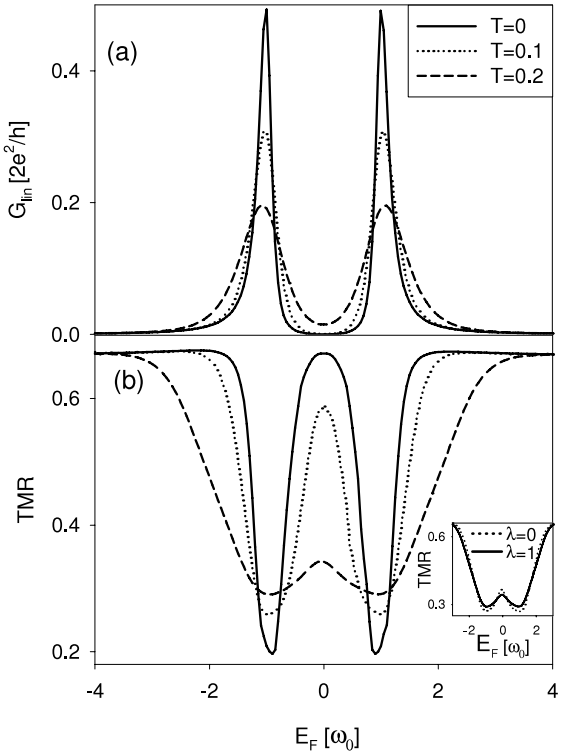

Figure 2. Linear conductance in the parallel configuration (a) and TMR (b) as a function of the lead Fermi energy level in the presence of electron–phonon coupling, $\lambda = 1$, and at different temperatures. The other parameters are as in figure 1. The inset in (b) shows differences between TMR calculated for $\lambda = 0$ (solid line, $\varepsilon_d = 1$, $U = 2$) and $\lambda = 1$ (dotted line, $\varepsilon_d = 0$, $U = 4$) at $T = 0.2$.

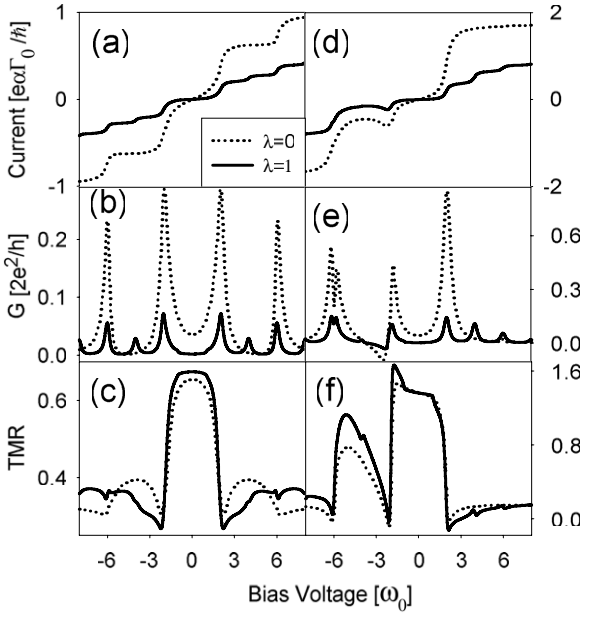

Figure 3. Bias dependence of the electric current, differential conductance and TMR for the symmetric ((a)–(c)) and asymmetric ((d)–(f)) junction in the parallel configuration. The current–voltage characteristics for the system without electron–phonon coupling (dotted curves) are compared to the case of strong electron–phonon coupling (solid curves). The parameters are $p_l = p_r = 0.5$, $\alpha = 1$ for the symmetric junction and $p_l = 0.4$, $p_r = 1$, $\alpha = 0.1$ for the asymmetric case. The other parameters are: $\widetilde{\varepsilon}_d = 1$, $\widetilde{U} = 2$ ($U = 4$ for $\lambda = 1$ and $U = 2$ for $\lambda = 0$), $\Gamma_0 = 0.2$, $V_g = 0$ and $T = 0$.

Figure 2 shows that thermal charge fluctuations lead to a reduction of the amplitude of the resonance peaks in the linear conductance as well as to reduction of the corresponding TMR minima. It is seen that with increasing temperature TMR approaches the Julliere value between the two dips indicating an occurrence of coherent tunneling processes through the discrete dot energy levels [42].

At a fixed temperature the Franck–Condon blockade only slightly enhances the TMR minima. Such a behavior is illustrated in the inset in figure 2(b), where a comparison of TMR for a non-phonon system, $\lambda = 0$, and for $\lambda = 1$ at $T = 0.2$ is displayed. The absence of the vibrational satellite peaks in the linear transport characteristics at $\lambda \neq 0$ confirms previous predictions within other theoretical approaches (see e.g. [19]). It is explained as the crucial consequence of the presence of Fermi seas in the leads, which gives rise to the so-called effect of 'floating' of phonon sidebands in the I–V curve at $V \approx 0$.

4.1.2. Nonlinear response regime, $V \neq 0$. Let us discuss now electronic transport in a nonequilibrium situation starting with the case of the symmetric junction at zero temperature, $T = 0$. The bias dependence of electric current, differential conductance as well as the corresponding TMR for such a system are shown in figures 3(a)–(c). When $\lambda = 0$, the current curve (dotted line in figure 3(a)) has a step-like profile with two steps appearing at threshold bias voltages at which the dot energy levels ε_d and $\varepsilon_d + U$ cross the Fermi level of the source electrode. Respectively, the differential conductance in figure 3(b) experiences two resonance peaks, whereas the corresponding TMR in figure 3(c) is significantly enhanced between the two thresholds. The central TMR peak in the bias voltage region, where the sequential tunneling current is exponentially suppressed, is due to higher-order tunneling processes, while the other TMR peaks come from differences of the sequential tunneling current in the parallel and antiparallel configurations of magnetic moments in the external electrodes.

When the hopping of electrons through the tunneling barriers is accompanied by the phonon cloud, then the exponential suppression of the tunneling rates gives rise to a suppression of the electric current in the whole bias voltage range. On the other hand, tunneling processes may be mediated by the phonon energy levels, which results in additional Frank–Condon steps in the current (solid line in figure 3(a)). Hence, due to a phonon emission at $T = 0$, vibrational sidebands in the differential conductance appear (figure 3(b)). The sidebands are spaced at the phonon energies from the main resonance peaks appearing at bias voltages at which $\widetilde{\varepsilon}_d$ and $\widetilde{\varepsilon}_d + \widetilde{U}$ enter the tunneling window. Moreover, figure 3(c) shows that when $\lambda \neq 0$, then TMR is enhanced below the first threshold bias voltage. This indicates that electron–phonon interactions increase the probability of additional higher-order tunneling processes that may occur in the bias voltage region where the sequential tunneling current is exponentially suppressed.

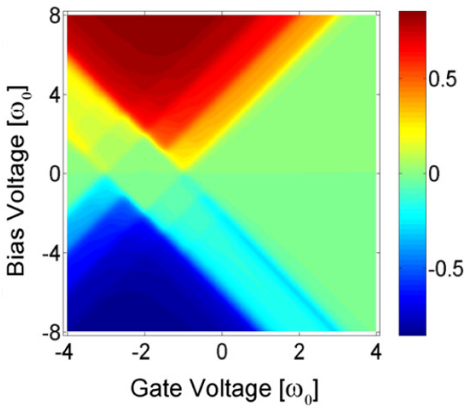

Figure 4. Map of tunneling current in the asymmetric junction in the parallel configuration, plotted as a function of the bias voltage and the bias gate voltage. The parameters are as in figure 3.

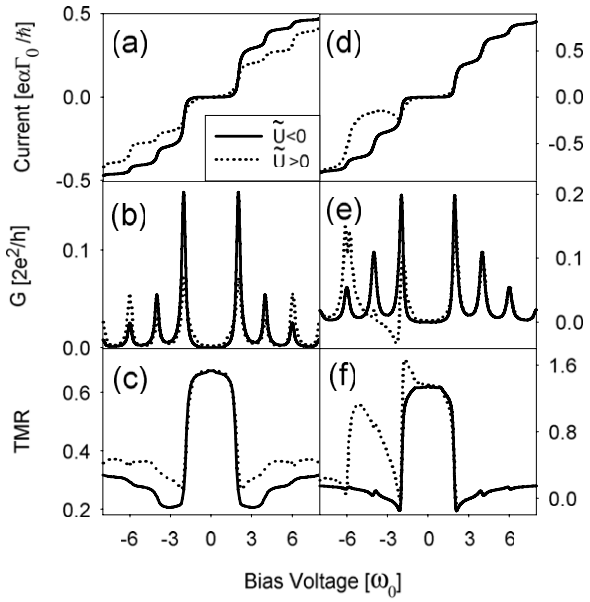

Figure 5. Bias dependence of the electric current, differential conductance and TMR for the symmetric ((a)–(c)) and asymmetric ((d)–(f)) junction in the parallel configuration and in the presence of strong electron–phonon interactions, $\lambda = 1$. The current–voltage characteristics for the system with positive effective charging energy, $\widetilde{U} = 2$, i.e. $U = 4$ (dotted curves) are compared to the case of negative effective charging energy, $\widetilde{U} = -2$, i.e. $U = 0$ (solid curves). The other parameters are as in figure 3.

The Franck–Condon blockade competing with the polaron-assisted electron transmission gives rise to TMR oscillations above the first threshold voltage. First, when the dot is singly occupied, the tunnel magnetoresistance oscillates below the TMR curve for the non-phonon system, whereas above the second threshold, when the dot becomes doubly occupied, it exceeds the TMR values calculated at $\lambda = 0$.

The basic transport property of the asymmetric tunneling junction is the asymmetry of its current–voltage characteristics with respect to the bias reversal. It is known that such a system may work as a mesoscopic diode [34–36]. The typical diode-like behavior in the tunneling junction with arbitrary Coulomb correlations on the dot and without electron–phonon interactions, $\lambda = 0$, is represented by the dotted curves in figures 3(d)–(f). For positive bias (the right lead is the source electrode), the current flows for both parallel and antiparallel configurations and thus TMR is significantly suppressed. In contrast, when electrons tunnel through the dot from the left electrode to the right (half-metallic) one, then below the first threshold voltage sequential tunneling is exponentially suppressed and only the higher-order tunneling processes are possible. At a sufficiently large bias voltage the energy level $\widetilde{\varepsilon}_{\mathrm{d}}$ ($\widetilde{\varepsilon}_{\mathrm{d}} = \varepsilon_{\mathrm{d}}$ at $\lambda = 0$) enters the tunneling window, and electric current starts to flow through the junction. However, this takes place only in a small voltage range in the vicinity of the first threshold voltage, where the resonant bump is observed. Above the bump, the current is suppressed by an electron residing on the dot and thus a negative differential conductance accompanied by a significant enhancement of TMR is observed between the two threshold bias voltages. Finally, when $\varepsilon_{\mathrm{d}} + U$ crosses the Fermi level of the source lead, the current increases again and finally saturates at a certain level.

In the presence of electron–phonon interactions, the electric current (solid line in figure 3(d)) has analogous features as in the symmetric case, i.e. the appearance of the Franck–Condon steps in the current is accompanied by a current suppression. The Franck–Condon blockade diminishes the height of the current steps and consequently reduces the height of the resonance peaks of the corresponding differential conductance (figure 3(e)). In the case considered here, the current suppression is asymmetric with respect to the bias reversal. Note first that, the magnitude of the current displayed for $\lambda = 1$ in figure 3(d), is still significant at $V > 0$ and comparable to the magnitude of the current flowing through the symmetric junction without electron–phonon interactions ($\lambda = 0$), which is shown in figure 3(a). Second, it is evident that the current suppression is much larger at negative than at positive bias. More specifically, when the dot is singly occupied at $V < 0$, then the electric current is almost entirely blocked for the assumed $\lambda = 1$. Thus, one may state that the polaron transmission may effectively enhance the diode-like behavior in asymmetric junctions with one half-metallic electrode. As also clearly seen in figure 3(f), when electron–phonon interactions are present, the tunnel magnetoresistance between the two thresholds is significantly enhanced at $V < 0$. This implies that phonon emission ($T = 0$) increases the probability of tunneling processes occurring in which one electron with spin antiparallel to the magnetization of the half-metallic (drain) lead is tunneling back to the source ferromagnetic electrode, while the second electron with the opposite spin, is tunneling to the drain electrode. Since in the parallel case there are more states to absorb in the drain half-metallic electrode, then such processes are more effective in P rather than in AP configuration, thus leading, in accordance with equation (38), to the observed enhancement of the TMR ratio.

The map in figure 4 shows in addition the dependence of the current rectification effect on the initial position of the dot energy level relative to the Fermi level of the external electrodes at $V = 0$. Until the dot is empty in equilibrium,

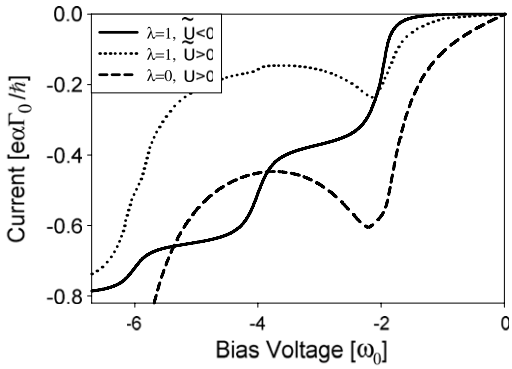

Figure 6. Comparison of the bias-dependent current for different values of $\widetilde{U}$ and λ in the asymmetric junction. The parameters are as in figures 3(d) and 5(d).

($eV_g > -\widetilde{\varepsilon}_d$), the current rectification results from the Coulomb blockade as well as from the current suppression between the two threshold bias voltages. By lowering the dot discrete level the dot may become singly ($-\widetilde{\varepsilon}_d \geqslant eV_g > -\widetilde{\varepsilon}_d - \widetilde{U}$) or doubly ($eV_g \leqslant -\widetilde{\varepsilon}_d - \widetilde{U}$) occupied in equilibrium. This way, by decreasing the bias gate voltage one increases the number of phonon energy levels that may become active in tunneling events, thus increasing the number of steps in the current. Simultaneously, the Franck–Condon blockade gives rise to enlargement of the diamond areas enclosed by the regions in the $eV - eV_g$ plane for which sequential tunneling processes take place.

4.2. *Negative effective Coulomb energy,* $\widetilde{U} < 0$

If the polaron shift leads to a negative effective charging energy, then the first step in the current in figure 5(a) appears at the bias voltage at which $\widetilde{\varepsilon}_d + \widetilde{U}$ crosses the Fermi level of the source electrode. Above this threshold the dot may be doubly occupied and thus, unlike in symmetric systems with $\widetilde{U} > 0$, the current enhancement is observed in the whole bias voltage range. For spin-polarized electronic transmission the difference between the quantities J_P and J_{AP} gives rise to

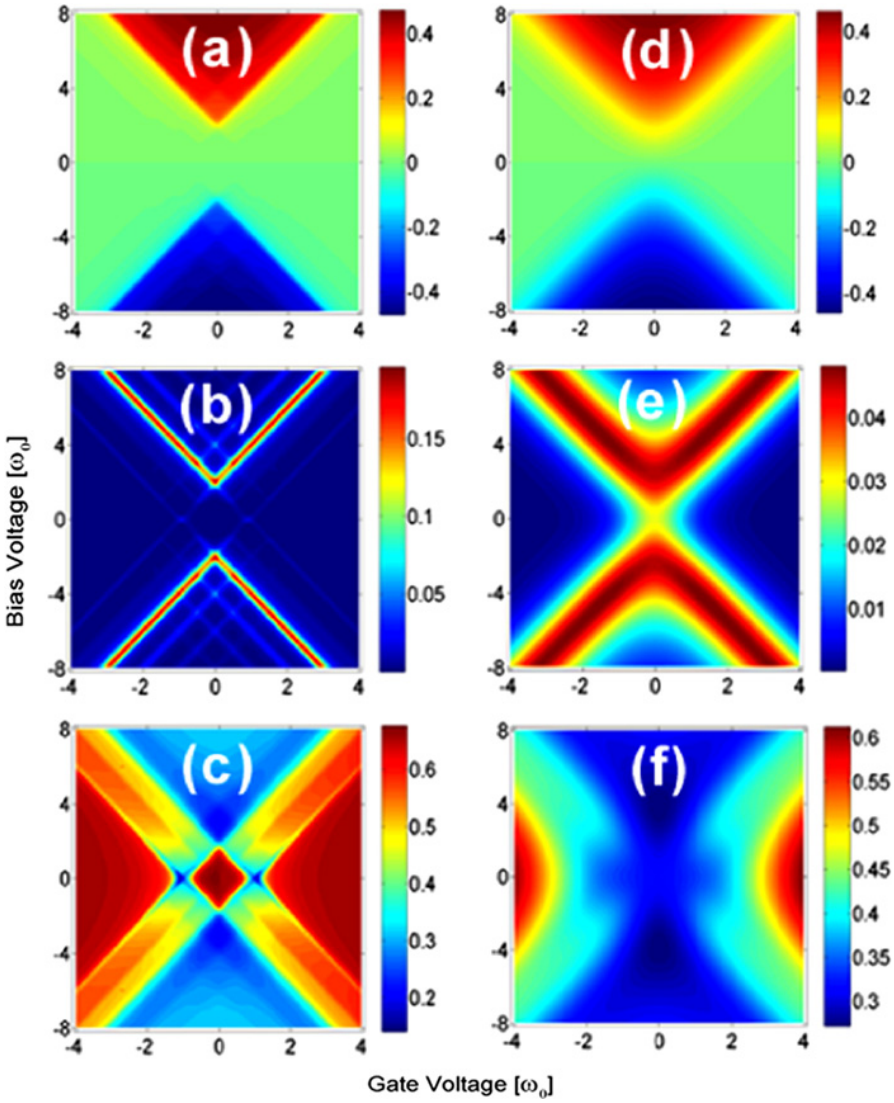

Figure 7. Maps of electric current ((a), (d)), differential conductance ((b), (e)) and TMR ((c), (f)) as a function of the transport bias voltage and the bias gate voltage. The curves are calculated for a symmetric junction in the parallel configuration, at two different temperatures, $T = 0$ ((a)–(c)) and $T = 0.5$ ((d)–(f)). The other parameters are: $p_l = p_r = 0.5$, $\alpha = 1$, $\widetilde{\varepsilon}_d = 1$, $U = -2$ ($U = 0$), $\Gamma_0 = 0.2$ and $T = 0$.

the suppression of TMR above the first threshold bias voltage illustrated in figure 5(c).

The magnitude of the current enhancement in systems with an asymmetric geometry strongly depends on the bias polarization. As shown in figure 5(d), above the first threshold at $V > 0$, the current–voltage characteristics evaluated for a negative $\widetilde{U}$ overlap with those obtained for a positive $\widetilde{U}$. In this case electrons are transmitted to the dot from the half-metallic electrode, which is fully spin-polarized in one direction. Then, regardless of the sign of the $\widetilde{U}$ parameter, above the first threshold only electrons with one spin orientation may be transmitted from the half-metallic source electrode to the dot.

The above situation is in contrast to the case of the negative bias, $V < 0$. As stated in the preceding subsection, if $\widetilde{U} > 0$, then above the first threshold the dot may be only singly occupied and current suppression, due to a down spin electron in the parallel configuration or an up spin electron in the antiparallel configuration, occurs until the energy level $\widetilde{\varepsilon}_\mathrm{d} + \widetilde{U}$ crosses the Fermi level of the source (ferromagnetic) lead. However when $\widetilde{U} < 0$, then above the first threshold the dot may become instantly doubly occupied, thus giving rise to enhancement of the current and consequently to a steep resonance peak in the differential conductance (figures 5(d) and (e)). The corresponding symmetric TMR in figure 5(f) results from the specific position of the dot discrete level $\widetilde{\varepsilon}_\mathrm{d} > 0$ relative to the Fermi level of the electrodes at $V = 0$, so that $\widetilde{\varepsilon}_\mathrm{d} + \widetilde{U} = -\widetilde{\varepsilon}_\mathrm{d}$.

In figure 6 a more detailed comparison of the behavior discussed in figures 3 and 5 for the electric current flowing through the asymmetric junction at negative bias voltages between the two thresholds is shown. Note that in contrast to the case of $\widetilde{U} > 0$, the diode-like behavior practically disappears and the rectification property is significantly diminished when the effective charging energy is negative. It is also seen that due to instantaneous double occupancy above the first threshold, the electric current at $\widetilde{U} < 0$ may even exceed the values calculated for the non-phonon system.

The temperature-dependent features of the considered tunneling junction are emphasized on maps in figure 7, where the electric current with a Franck–Condon blockade as well as Coulomb blockade areas is shown in the plane $eV - eV_\mathrm{g}$, together with the corresponding differential conductance and TMR. There, numerical results for symmetric junctions in the parallel configuration and at zero temperature are compared to those obtained at $T = 0.5$. It is seen that washing out of the Frank–Condon steps in the current is accompanied by vanishing oscillations of TMR. Figure 7(e) shows also that with increasing temperature broad phonon absorption peaks appear in the differential conductance in the Coulomb blockade region. The supplementary cross sections in figure 8, taken at $eV_\mathrm{g} = 1$, show in more detail a thermal sensitivity of the polaronic oscillations of the conductance and the TMR quantity.

5. Summary and conclusions

Using the nonequilibrium Green function approach we have considered tunneling through an interacting single-level quantum dot coupled to ferromagnetic leads, in the presence of electron–phonon interactions. Phonon emission and absorption spectra calculated for different temperatures show that in both linear and nonlinear response regimes spin-polarized electron transmission may be mediated by the phonon energy levels. These tunneling processes are accompanied by renormalization of the dot energy level as well as by appearance of vibrational sidebands spaced at the phonon energy. In a nonequilibrium situation a strong enough electron–phonon coupling leads to a step-like electric current behavior with the Franck–Condon steps occurring at the threshold bias voltages at which phonon-assisted electron transmission takes place. Consequently, TMR oscillations in nonlinear response regime have been observed.

If the effective charging energy is positive, $\widetilde{U} > 0$, then in symmetric systems the exponential suppression of the tunneling rates give rise to a suppression of the spin-polarized current in the whole bias voltage range as well as to an enhancement of the oscillatory behavior of TMR above the threshold bias voltage at which the discrete dot energy level enters the tunneling window. Surprisingly, however, it is found that for asymmetric junctions with one electrode being half-metallic, the diode-like features may be effectively enhanced when the tunneling processes due to electron–phonon interactions start to increase the current suppression. Consequently, the current rectification effect becomes more prominent in the presence of the Franck–Condon blockade, which, besides the multiplied step-like current–voltage dependence, gives rise to an enlargement of the Coulomb blockade diamonds in the electric current characteristics in the eV–eV_g plane.

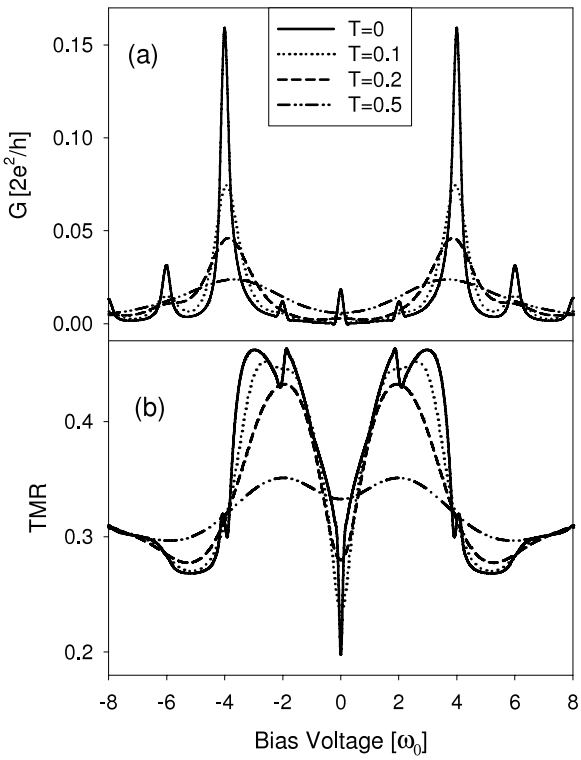

Figure 8. Bias dependence of the differential conductance (parallel configuration) (a) and TMR (b) for selected temperatures and for $eV_\mathrm{g} = 1$. The other parameters are as in figure 6.

When the polaron shift leads to a negative effective charging energy, $\widetilde{U} < 0$, then the sequential tunneling processes through the doubly occupied dot competing with the Franck–Condon blockade mechanism give rise, in contrast to the positive-$\widetilde{U}$ case, to current enhancement beyond the Coulomb blockade regime in both symmetric as well as asymmetric junctions. The latter feature leads also to a significant reduction of the diode-like behavior in asymmetric tunneling junctions with one half-metallic electrode.

With increasing temperature, the essential feature of spin-polarized polaronic transport, i.e. oscillations of TMR, are diminished and eventually disappear in the nonequilibrium situation at sufficiently small gate bias voltages. This process is accompanied by a washing out of the Franck–Condon steps in the current as well as by a broadening and diminishing of the satellite resonance peaks in the differential conductance. On the other hand, for $T > 0$ inelastic cotunneling leads to the appearance of vibrational absorption sidebands inside the Coulomb blockade region. Thus, even at higher temperatures a phonon-induced oscillatory TMR behavior may be observed.

Acknowledgment

This work was supported by funds of the Polish Ministry of Science and Higher Education as a research project in years 2006–2009.

References

[1] Fujisawa T, Oosterkamp T H, van der Wiel W G, Broer B W, Aguado R, Tarucha S and Kouwenhoven L P 1998 *Science* **282** 932
[2] Park H, Park J, Lim A K L, Anderson E H, Alivisatos A P and McEuen P L 2000 *Nature* **407** 57
[3] Qin H, Holleitner1 A W, Eberl K and Blick R H 2001 *Phys. Rev.* B **64** 241302
[4] Park J, Pasupathy A N, Goldsmith J I, Chang C, Yaish Y, Petta J R, Rinkoski M, Sethna J P, Abruña H D, McEuen P L and Ralph D C 2002 *Nature* **417** 722
[5] Zhitenev N B, Meng H and Bao Z 2002 *Phys. Rev. Lett.* **88** 226801
[6] Yu L H and Natelson D 2004 *Nano Lett.* **4** 79
[7] Qiu X H, Nazin G V and Ho W 2004 *Phys. Rev. Lett.* **92** 206102
[8] Weig E M, Blick R H, Brandes T, Kirschbaum J, Wegscheider W, Bichler M and Kotthaus J P 2004 *Phys. Rev. Lett.* **92** 046804
[9] LeRoy B J, Lemay S G, Kong J and Dekker C 2004 *Nature* **432** 371
[10] Yu L H, Keane Z K, Ciszek J W, Cheng L, Stewart M P, Tour J M and Natelson D 2004 *Phys. Rev. Lett.* **93** 266802
[11] Wingreen N S, Jacobsen K W and Wilkins J W 1989 *Phys. Rev.* B **40** 11834
[12] Haug H and Jauho A-P 1996 *Quantum Kinetics in Transport and Optics of Semiconductors* (Berlin: Springer)
[13] Kuo D M-T and Chang Y C 2002 *Phys. Rev.* B **66** 085311
[14] Urban L and McKenzie R H 2002 *Phys. Rev.* B **66** 075303
[15] Alexandrov A S and Bratkovsky A M 2003 *Phys. Rev.* B **67** 235312
[16] Flensberg K 2003 *Phys. Rev.* B **68** 205323
[17] Zhu J-X and Balatsky A V 2003 *Phys. Rev.* B **67** 165326
[18] Braig S and Flensberg K 2003 *Phys. Rev.* B **68** 205324
[19] Mitra A, Aleiner I and Millis A J 2004 *Phys. Rev.* B **69** 245302
[20] Chen Z-Z, Rong L and Zhu B-f 2005 *Phys. Rev.* B **71** 165324
[21] Koch J and von Oppen F 2005 *Phys. Rev. Lett.* **94** 206804
[22] Koch J, Raikh M E and von Oppen F 2006 *Phys. Rev. Lett.* **96** 056803
[23] Koch J, von Oppen F and Andreev A V 2006 *Phys. Rev.* B **74** 205438
[24] Galperin M, Nitzan A and Ratner M A 2006 *Phys. Rev.* B **73** 045314
[25] Wang R-Q, Zhou Y-Q, Wang B and Xing D Y 2007 *Phys. Rev.* B **75** 045318
[26] Galperin M, Nitzan A and Ratner M A 2007 *Phys. Rev.* B **76** 035301
[27] Zazunov A and Martin T 2007 *Preprint* cond-mat/0703626
[28] Moodera J S, Kinder L R, Wong T M and Meservey R 1995 *Phys. Rev. Lett.* **74** 3273
[29] Parkin S S P, Roche K P, Samant M G, Rice P M, Beyers R B, Scheuerlein R E, O'Sullivan E J, Brown S L, Gucchigano J, Abraham D W, Lu Y, Rooks M, Trouilloud P L, Wanner R A and Gallagher W J 1999 *J. Appl. Phys.* **88** 5828
[30] Zhang X, Li B S, Sun G and Pu F C 1997 *Phys. Rev.* B **56** 5484
Wilczyński M and Barnaś J 2000 *J. Magn. Magn. Mater.* **221** 373
[31] Barnaś J and Fert A 1998 *Phys. Rev. Lett.* **80** 2058
Barnaś J and Fert A 1998 *Europhys. Lett.* **44** 85
[32] Takahashi S and Maekawa S 1998 *Phys. Rev. Lett.* **80** 1758
[33] Brataas A, Nazarov Yu V, Inoue J and Bauer G E W 1999 *Eur. Phys. J.* B **9** 421
Wang X H and Brataas A 1999 *Phys. Rev. Lett.* **83** 5138
[34] Bułka B R 2000 *Phys. Rev.* B **62** 3186
[35] Rudziński W and Barnaś J 2001 *Phys. Rev.* B **69** 085318
[36] Souza F M, Euges J C and Jauho A P 2007 *Phys. Rev.* B **75** 166303
[37] Świrkowicz R, Barnaś J and Wilczyński M 2002 *J. Phys.: Condens. Matter* **14** 2011
[38] Fransson J, Eriksson O and Sandalov I 2002 *Phys. Rev. Lett.* **88** 226601
[39] Bułka B R and Lipiński S 2003 *Phys. Rev.* B **67** 024404
[40] Lopez R and Sanchez D 2003 *Phys. Rev. Lett.* **90** 116602
[41] Braun M, König J and Martinek J 2004 *Phys. Rev.* B **70** 195345
[42] Weymann I, König J, Martinek J, Barnaś J and Schön G 2005 *Phys. Rev.* B **72** 115334
[43] Weymann I, Barnaś J, König J, Martinek J and Schön G 2005 *Phys. Rev.* B **72** 113301
[44] Rudziński W, Barnaś J, Świrkowicz R and Wilczyński M 2005 *Phys. Rev.* B **71** 205307
[45] Weymann I and Barnaś J 2006 *Phys. Rev.* B **73** 205309
[46] Świrkowicz R, Wilczyński M, Wawrzyniak M and Barnaś J 2006 *Phys. Rev.* B **73** 193312
[47] Imamura H, Chiba J, Mitani S, Takanashi K, Takahashi S, Maekawa S and Fujimori H 2000 *Phys. Rev.* B **61** 46
[48] Yakushiji K, Mitani S, Takanashi K, Takahashi S, Maekawa S, Imamura H and Fujimori H 2001 *Appl. Phys. Lett.* **78** 515
[49] Mahan G D 2000 *Many-Particle Physics* (New York: Plenum)
[50] Jauho A-P, Wingreen N S and Meir Y 1994 *Phys. Rev.* B **50** 5528